The Journal of Immunology

Two Structurally Different Rituximab-Specific CD20 Mimotope Peptides Reveal That Rituximab Recognizes Two Different CD20-Associated Epitopes

Federico Perosa, Elvira Favoino, Chiara Vicenti, Andrea Guarnera, Vito Racanelli, Vito De Pinto and Franco Dammacco

J. Immunol. 2009;182;416-423
http://www.jimmunol.org/cgi/content/full/182/1/416

The Journal of Immunology is published twice each month by The American Association of Immunologists, Inc., 9650 Rockville Pike, Bethesda, MD 20814-3994.

Print ISSN: 0022-1767 Online ISSN: 1550-6606.

Two Structurally Different Rituximab-Specific CD20 Mimotope Peptides Reveal That Rituximab Recognizes Two Different CD20-Associated Epitopes[1]

Federico Perosa,[2]* Elvira Favoino,* Chiara Vicenti,* Andrea Guarnera,† Vito Racanelli,* Vito De Pinto,† and Franco Dammacco*

Peptide mimotopes of the CD20 epitope recognized by rituximab are useful tools for studying this therapeutic mAb's functional properties. We previously identified two structurally different peptides that are both effective mimotopes: a 7-mer cyclic peptide (Rp15-C) bearing the antigenic motif ⟨a/sNPS⟩ that matches ^{170}⟨ANPS⟩^{173} of the extracellular loop of CD20, and a 12-mer linear peptide (Rp5-L) containing the antigenic motif ⟨WPxWLE⟩ lacking sequence homology to CD20. In this study, we investigated whether the different structures of Rp15-C and Rp5-L reflect the mimicry of the same or different CD20 epitopes recognized by rituximab. Using immunochemical methods, we found that, like Rp15-C, Rp5-L mimics the raft-associated form of CD20 (by inhibiting rituximab binding to CD20 in vitro). Rp5-L and Rp15-C elicit, in immunized mice, anti-CD20 Abs that stain CD20$^+$ cells with a punctate pattern similar to that of rituximab. However, only anti-Rp5-L Abs recognize denatured CD20. When phage-display peptide libraries were panned with anti-Rp5-L, phage clones were enriched that expressed the consensus qWPxwL, similar to the antigenic motif ⟨WPxWLE⟩, but not matching ⟨a/sNPS⟩. Finally, ⟨WPxWLE⟩ and ⟨ANPS⟩ share some, but not all, contact sites within the rituximab Ag-combining site, indicating that ⟨WPxWLE⟩ is not an exact replica of Rp15-C (or CD20) ⟨ANPS⟩. Altogether, these results indicate that the two structurally different peptides are also conformationally different, and suggest that rituximab recognizes two different CD20-associated epitopes. ***The Journal of Immunology,*** **2009, 182: 416–423.**

The CD20 is a 30- to 35-kDa integral membrane protein expressed by B lymphocytes in early stages of differentiation and by most B cell lymphomas, but not by differentiated plasma cells (1). This B cell-associated Ag has been successfully targeted with the cytotoxic chimeric mAb rituximab, which improves the effects of conventional treatment for B cell tumors (2–4) and autoimmune diseases (5, 6). CD20 is associated with membrane raft microdomains and, when bound by rituximab, it activates transmembrane signaling pathways (1); one manifestation of this activation is the transient production of ceramide in membrane rafts (7). Although the crystal structure of CD20 has not been defined, the protein is believed to be a tetraspan molecule with intracellular termini and two extracellular loops of 9 and 43 residues spanning from aa 72 to 80 and from aa 142 to 184, respectively (8, 9). The larger extracellular loop, particularly nearby or between residues A^{170} and S^{173}, contains the epitope recognized by rituximab and most other anti-CD20 mAbs (10). The binding of rituximab is abolished by reduction and alkylation of CD20, indicating that the recognized epitope is conformational (11). However, despite apparently similar specificity, rituximab and other anti-CD20 mAbs have different effector functions and different efficacies (12).

Peptide mimics of the CD20 epitope recognized by rituximab have been isolated and characterized (13, 14) to understand differences in the fine specificities of rituximab and other anti-CD20 mAbs (12). Moreover, there is clinical interest in studying such peptide mimotopes, because those that can stimulate an anti-CD20 response in the immunized host have potential use as active immunotherapy reagents (13, 15, 16). A peptide-based active immunotherapy may reduce a patient's need for multiple infusions, as are common with anti-CD20, and would avoid the risk of Ab production to the nonhuman part or idiotypic region of the therapeutic mAb (17, 18). Finally, understanding the antigenic and immunogenic properties of these mimotopes may help design effective peptide-based therapies (19).

We recently characterized a panel of cyclic and linear peptides specifically reacting with rituximab (13). The peptides were isolated by screening three phage-display peptide libraries (PDPLs),[3] expressing 7-mer cyclic (cysteine-constrained) and 7- and 12-mer linear peptides. The cyclic peptides isolated by screening with rituximab contained the rituximab-specific antigenic motif ⟨**a/sNPS**⟩ (motif amino acids are in bold), which corresponds to the ^{170}ANPS^{173} stretch of the larger exposed loop of CD20. The linear peptides contained the consensus motif ⟨**WPxWLE**⟩, which did not match any portion of CD20. Representative synthetic peptides Rp15-C (cyclic) and Rp5-L (linear) inhibited rituximab binding to CD20$^+$ cells in a specific, dose-dependent manner and, in immunized mice, generated Abs with specificity and effector functions similar to rituximab (13).

The mechanisms by which two structurally distinct peptides—a cyclic one matching a four-residue motif in the large extracellular

*Department of Internal Medicine and Clinical Oncology, University of Bari Medical School, Bari, Italy; and †Department of Chemical Sciences, Section of Molecular Biology, University of Catania, Catania, Italy

Received for publication September 8, 2008. Accepted for publication October 28, 2008.

The costs of publication of this article were defrayed in part by the payment of page charges. This article must therefore be hereby marked *advertisement* in accordance with 18 U.S.C. Section 1734 solely to indicate this fact.

[1] This work was supported by a grant (2007–2008) from Associazione Italiana per la Ricerca sul Cancro, Milan, Italy.

[2] Address correspondence and reprint requests to Dr. Federico Perosa, Department of Internal Medicine and Clinical Oncology, University of Bari Medical School, Piazza G. Cesare 11, I-70124 Bari, Italy. E-mail address: f.perosa@dimo.uniba.it

[3] Abbreviations used in this paper: PDPL, phage-display peptide library; CTB, cholera toxin subunit B; KLH, keyhole limpet hemocyanin.

loop of CD20 and a linear one lacking sequence homology to CD20—have similar mimotopic properties are not known. One possibility is that the tertiary structure of Rp5-L conformationally mimics the ⟨ANPS⟩ epitope; peptides with these discontinuous or conformational epitopes have already been characterized for other Ags (20–23). Alternatively, the two peptides could mimic a single epitope in different conformational states; in fact, CD20 has recently been found to associate more tightly with membrane rafts upon Ab binding, possibly due to a conformation change (24). We have already shown, using double immunofluorescence binding and ceramide synthesis assays, that Rp15-C mimics membrane raft-associated CD20 (19), but this information is not yet available for Rp5-L. A third possibility is that the peptides mimic two distinct, but spatially close CD20-associated epitopes. In this study, we investigated which of these possible molecular mechanisms most likely explains the different properties of Rp5-L and Rp15-C, with the aims of better understanding the functional properties of rituximab as well as the ability of peptides to mimic conformational epitopes of therapeutic importance.

Materials and Methods

Animals and cells

The animal studies were reviewed and approved by the ethical review committee of the University of Bari Medical School. Female BALB/c mice (8–12 wk old) were purchased from Charles River Breeding Laboratory.

The human $CD20^-$ T lymphoid cell line CEM and the human $CD20^+$ B lymphoid cell lines Raji and Daudi, established models for exploring rituximab's reactivity and functions (7, 25), were grown in RPMI 1640 medium supplemented with 10% FCS (HyClone) and 5 mM L-glutamine.

Reagents, Abs, and peptides

Electrophoresis reagents were purchased from Bio-Rad. Unless otherwise specified, all other chemicals were purchased from Sigma-Aldrich.

PE-conjugated streptavidin (PE-streptavidin) was purchased from BD Biosciences; cholera toxin subunit B (CTB) and biotin-*N*-hydroxysuccinimide ester were purchased from Sigma-Aldrich; CTB was coupled to biotin, as previously described (26).

Anti-CD20 chimeric (IgG1) mAb rituximab and the isotype-matched anti-TNF-α mAb infliximab were purchased from Roche Pharmaceuticals and Centocor, respectively. Mouse anti-ceramide mAb MID 15B4 (IgM) was purchased from Alexis. HRP-conjugated mouse mAb to bacteriophage M13 major coat protein product of gene VIII (HRP-anti-M13 Ab) was purchased from GE Healthcare Bio-Sciences. Purified rabbit IgG, HRP- and FITC-conjugated goat anti-human and anti-mouse IgG (Fc portion), and FITC-conjugated goat anti-mouse IgM were purchased from Jackson ImmunoResearch Laboratories.

Cyclic and linear peptides were synthesized by Primm. Their quality was checked by analytical reverse-phase chromatography and mass spectral analysis, and their purity was >80%. Synthetic peptides included the following: the rituximab-specific 7-mer linear peptide Rp1-L (**WPRWLE**N; motif amino acids are in bold), 12-mer linear peptide Rp5-L (QDKLTQ**WPKWLE**), and cysteine-constrained 7-mer cyclic peptide Rp15-C (ACPY**ANPS**LC) (13); the anti-HLA class I mAb HC-10-specific peptide Qp-1a (QEG**P**EY**WDR**NT) (27); and the CD20-derived 20-mer linear peptide RpCD20-L (YNCEP**ANPS**EKNSPSTQYCY) corresponding to residues 165–184 of the extracellular loop of CD20 (13).

Rituximab binding and activation of ceramide synthesis in $CD20^+$ cells

To test the ability of peptide mimotopes to inhibit the binding of rituximab to native CD20, rituximab (2.5 μg/ml in PBS; 60 μl) was preincubated with an equal volume of PBS containing 100 μg/ml Rp5-L, Rp15-C, Qp-1a, or no peptide, for 1 h at 4°C. Then, 100 μl of the rituximab-peptide solution was added to Raji cells (1×10^6/50 μl) previously treated with rabbit IgG to block FcR binding sites. Following a 10-min incubation at 37°C, cells were washed once with 4 ml of PBS containing 0.5% BSA (PBS-BSA), and fixed with 2% paraformaldehyde for 15 min at 25°C. Cells were washed once with PBS-BSA, pelleted, and then incubated in 50 μl of biotinylated CTB (10 μg/ml), to reveal membrane rafts, for 30 min on ice. Cells were washed once with PBS-BSA, and incubated with PE-streptavidin (1:500) and FITC-conjugated anti-human IgG (1:100) in PBS for 30 min at 4°C. Cells were washed with PBS-BSA, mounted on glass coverslips with polyvinyl alcohol mounting medium with Dabco (Sigma-Aldrich), and examined with a Nikon confocal microscope using a ×60 Plan Apo VC objective. An argon laser at 488 nm was used to excite FITC, and a helium-neon laser was filtered at 560 nm to excite PE.

The ability of peptide mimotopes to inhibit rituximab-induced membrane ceramide synthesis in Daudi cells was tested, as described elsewhere (7), with minor modifications. Briefly, 50 μl of rituximab (10 μg/ml in PBS) was preincubated for 1 h at 4°C with an equal volume of PBS containing Rp5-L (400, 40, or 4 μg/ml), Qp-1a (400 μg/ml), or no peptide. The rituximab-peptide solution (100 μl) was added to Daudi cells (1×10^6/50 μl), incubated for 10 min at 37°C, fixed with 2% paraformaldehyde for 15 min at 25°C, washed with PBS-BSA, and resuspended in 50 μl of rabbit IgG (50 mg/ml in PBS) for 30 min at 4°C. After an additional wash, ceramide production was revealed by sequential incubation of cells with anti-ceramide IgM (1:100) for 30 min at 4°C, followed by FITC-conjugated anti-mouse IgM (1:100). The fluorescent profiles of labeled cells were documented with a FACScan cytofluorimeter.

Antipeptide antisera generation, specificity testing, and purification

Peptides Rp5-L, Rp15-C, RpCD20-L, and Qp-1a were coupled to carrier protein keyhole limpet hemocyanin (KLH) or BSA using glutaraldehyde, as described previously (13). BALB/c mice (five mice per peptide) were immunized, as described previously (19), using 1 μg of KLH peptide for priming and for boosting on days 7, 14, 21, and 28. An additional two BALB/c mice were immunized with KLH only. Sera were harvested on day 28 and every week thereafter up to day 56, and tested for specificity in an ELISA. Briefly, 96-well polyvinyl chloride microtiter plates were coated with 50 μl of PBS containing 10 μg/ml BSA-conjugated peptide for 12 h at 4°C. Wells were washed once with PBS containing 0.05% Tween 20 (PBS-T20) and blocked with PBS-BSA. Antipeptide sera were added to the plates in 10-fold serial dilutions (starting from a 1/10 dilution) and incubated for 4 h at 25°C. Wells were washed three times with PBS-T20, and bound IgG was detected with HRP-conjugated anti-mouse IgG (Fc portion; 1:2000) and *o*-phenylenediamine (0.5 mg/ml); color development was stopped by adding 100 μl of 2 N H_2SO_4 and was read at 492 nm. Background binding was determined from the absorbance in wells that were not incubated with sera.

Using this ELISA, sera drawn from days 35 to 56 were found to display the highest titer to the corresponding immunogen in all animals. The same sera were used for immunofluorescence staining of cells to screen for mice that had developed $CD20^+$ cell-reacting Abs, as described (19); two mice immunized with Rp5-L and two with Rp15-C developed $CD20^+$ cell-reacting Abs. Sera drawn on days 35, 42, 49, and 56 from each pair of mice were pooled for use in confocal immunofluorescence, Western blotting, and the purification of peptide-specific IgG by precipitation with caprylic acid (19, 28). These IgG preparations were cleared of anti-KLH IgG, as described (19). Their purity was shown on Coomassie-stained SDS-PAGE. Protein concentration was measured with the bicinchoninic acid assay (Pierce). Their specificities were tested and compared with that of rituximab and infliximab (negative control) by ELISA, as described in the previous paragraph, using KLH peptide as coating reagent; in assays using rituximab and infliximab, the secondary Ab was HRP-conjugated anti-human IgG.

Specificity of binding of antipeptide antisera to CD20

The binding of antipeptide antisera to $CD20^+$ Raji and $CD20^-$ CEM cells was tested in a confocal immunofluorescence binding assay similar to that described previously for rituximab. Briefly, 50 μl of antipeptide antisera (diluted 1/20 in PBS-BSA) or rituximab (2.5 μg/ml in PBS) was added to rabbit IgG-pretreated Raji or CEM cells (5×10^5 cells in 50 μl of PBS). The cells were incubated at 4°C for 30 min, washed once with ice-cold PBS-BSA, and labeled with FITC-conjugated anti-mouse or anti-human IgG (Fc portion, 1:100). Cells were washed, fixed, and mounted for confocal microscopy, as described earlier.

To test the ability of immunogenic peptides to inhibit binding, 50 μl of antipeptide antiserum (diluted 1/20 in PBS-BSA) was preincubated with an equal volume of PBS containing Rp5-L or Rp15-C (400, 40, or 4 μg/ml), Qp-1a (400 μg/ml), or no peptide for 1 h at 4°C; background binding was determined using anti-KLH antiserum (1/20 in PBS) or just FITC secondary Ab. The Ab solution (100 μl) was added to Raji cells (5×10^5/50 μl), which were incubated for 30 min at 4°C, washed once with ice-cold PBS-BSA, and resuspended in 50 μl of FITC-conjugated anti-mouse IgG (Fc portion, 1:100). Immunofluorescence was measured using a FACScan cytofluorimeter.

The specificity of antipeptide antisera for denatured CD20 was characterized by Western blotting. Briefly, lysed Raji cells (1×10^8 cells/ml) were

immunoprecipitated with rituximab (for CD20) or infliximab (negative control), as described (10). In some cases, cell lysates were preadsorbed with rituximab by three incubations, each for at least 2 h at 4°C, with protein G-Sepharose (10 μl of packed resin) coupled to rituximab (10 μg). Immunoprecipitated proteins were eluted in SDS sample buffer, separated by SDS-PAGE under reducing conditions, and transferred to polyvinylidene fluoride membranes. Western blotting was done using anti-Rp5-L antiserum (1:50) or anti-RpCD20-L (1:50) and HRP-conjugated anti-mouse IgG as secondary Ab; bound Abs were revealed with diaminobenzidine.

Affinity selection, immunoscreening, and sequence analysis

The PDPLs expressing 7-mer cyclic (Ph.D.-C7C) and 12-mer linear (Ph.D.-12) peptides were purchased from New England Biolabs. PDPLs were panned with purified mouse anti-Rp5-L IgG, according to the manufacturer's instructions and as described (27); mouse anti-KLH IgG was used to remove phage particles binding to isotypic and allotypic determinants. Anti-Rp5-L IgG-specific phage clones were detected with anti-M13 mAb, as described (27). Selected phage particles were amplified in *Escherichia coli*, and the supernatant fluids of 30 randomly selected colonies were tested in ELISA for specificity to anti-Rp5-L IgG, as described (19). Nucleotide sequences of phage clone inserts specific for anti-Rp5-L were determined according to the manufacturer's instructions, at the Primm sequencing facility (Naples, Italy). Multiple sequence alignments were performed with MULTALIN at Pôle BioInformatique Lyonnaise (http://npsa-pbil.ibcp.fr/cgi-bin/npsa_automat.pl?page=/NPSA/npsa_multalin.html).

Computer modeling and docking analysis

Peptide structure was modeled using the SP4 Fold Recognition server (http://sparks.informatics.iupui.edu/SP4/). To minimize the interference of amino acids not essential for binding, Rp5-L was replaced with Rp1-L (^{1}**WP**R**WLE**N^{7}), which is the shortest rituximab-reacting peptide bearing the Rp5-L motif ⟨WPxWLE⟩ (13). Only the model with the best *Z* score was considered (29).

Then, Rp1-L was docked to rituximab Fab (Brookhaven Protein Data Bank entry: 2OSL) (30) using the rigid body algorithm ZDOCK 3.0 (31). To improve the sampling accuracy, the docking site was restricted to part of the Fab region. A distance of 4 Å from the sequence ^{170}ANPS^{173} of CD20 defined the docking grid. The set of 2000 poses obtained was then clustered with a 0.3 Å threshold, following a clustering algorithm (32). The best model of the rituximab-Rp1-L complex arising from clustering, i.e., that with the highest ZDOCK score, was first introduced into an explicit solvent box and then energy minimized with the Chemistry at Harvard Molecular Mechanics force field (33), using 3000 steps of the deepest descent, followed by adopted basis Newton-Raphson minimization. No restraint was applied to either the protein/peptide or the solvent structure. PyMOL v.1.0 (34) was used for visualization and rendering.

Computer visualization of rituximab-Fab in complex with the ⟨ANPS⟩ motif of the extracellular loop of CD20 was based on the published crystal structure (30).

Results

Rp5-L mimics raft-associated CD20

To determine whether the peptide mimotope Rp5-L mimics raft-associated (functional) CD20, as previously shown for Rp15-C (19), we performed immunofluorescence binding assays on Raji CD20^{+} cells doubly labeled for raft microdomains and bound rituximab (Fig. 1*A*). Incubation of rituximab with Raji cells in the absence of inhibitor peptide generated a punctate staining pattern indicative of binding to CD20 in raft microdomains (data not shown). Preincubation of rituximab with Rp5-L, like Rp15-C, completely abolished rituximab binding, whereas staining of raft microdomains was maintained. Preincubation of rituximab with unrelated peptide Qp-1a had no effect on binding; the yellow punctate staining of the merged double fluorescence image indicated colocalization of CD20 and raft microdomains. This mimicry by Rp5-L of a functional CD20 epitope was further assessed with a ceramide synthesis assay (Fig. 1*B*). Stimulation of Daudi cells with rituximab alone (data not shown) or in the presence of unrelated peptide Qp-1a resulted in a strong right shift in the fluorescent profile of the cells, indicative of the production of ceramide in the plasma membrane. Preincubation of rituximab with increasing concentrations of Rp5-L inhibited ceramide production in a dose-dependent manner. Together, these data document that Rp5-L specifically blocks CD20 binding and activation by rituximab, and suggest that, like Rp15-C, Rp5-L is an antigenic mimic of raft-associated CD20.

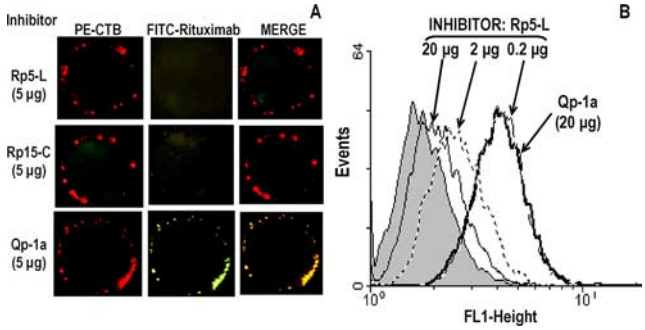

FIGURE 1. Inhibition by peptide mimotopes Rp5-L and Rp15-C of rituximab binding to raft-associated CD20 (*A*) and of rituximab-stimulated increase in membrane ceramide (*B*) in human CD20^{+} B lymphoid cells. *A*, Both Rp5-L and Rp15-C, but not unrelated Qp-1a, inhibit binding of rituximab to CD20 associated with raft microdomains, seen as punctate staining. Rituximab (2.5 μg/ml in PBS; 60 μl) was preincubated with an equal volume of PBS containing 100 μg/ml Rp5-L (63.6 μM), Rp15-C (96.3 μM), Qp-1a (71.7 μM), or no peptide. The rituximab-peptide solution (100 μl) was added to Raji cells (1×10^6/50 μl), which were incubated for 10 min at 37°C, washed, and fixed with paraformaldehyde. Cells were washed and incubated with biotinylated CTB to label raft microdomains, and then washed and labeled with FITC-conjugated anti-human IgG (to detect rituximab) and PE-conjugated streptavidin (to detect CTB). Cells were examined by confocal microscopy with excitation at 488 nm (FITC) and at 560 nm (PE). Data are representative of three independent experiments. Five micrograms of Rp5-L, Rp15-C, and Qp-1a are 3.2, 4.8, and 3.6 nmol, respectively. *B*, Rp5-L specifically inhibits rituximab-stimulated increase in ceramide. Rituximab (10 μg/ml in PBS; 50 μl) was preincubated with an equal volume of PBS containing 400, 40, or 4 μg/ml Rp5-L or Qp-1a (400 μg/ml equals 254.5 μM Rp5-L and 286.9 μM Qp-1a). The rituximab-peptide solution was added to Daudi cells (1×10^6/tube), which were incubated for 10 min at 37°C, washed, fixed with paraformaldehyde, and treated with rabbit IgG (50 μg/ml) for 30 min at 4°C to block FcR binding sites. Ceramide production induced by rituximab was measured by incubating cells with anti-ceramide mAb, followed by labeling with FITC-conjugated anti-mouse IgM. Immunofluorescence was measured with a FACScan cytofluorimeter. Background fluorescence profile of cells (without rituximab treatment) is indicated (shaded area). Data are representative of three independent experiments. Twenty micrograms of Rp5-L and Qp-1a are 12.7 and 14.4 nmol, respectively.

Fine specificities of CD20-specific anti-Rp5-L and anti-Rp15-C Abs are different

To determine whether Rp5-L and Rp15-C mimic the same or different epitopes of CD20, we investigated the fine specificities of the corresponding Abs generated in immunized mice. First, the fluorescence staining patterns of anti-Rp5-L and anti-Rp15-C antisera, compared with that of rituximab, were determined on CD20^{+} Raji cells and CD20^{-} CEM cells (Fig. 2). Immunofluorescence staining of Raji cells by antipeptide sera and by rituximab resulted in a punctate pattern, typical of the staining of raft-associated CD20. Staining of CEM cells was negative, indicating that the labeling of Raji cells was in all cases specific for CD20.

Then, the paratope specificities of the antipeptide antisera were assessed in an immunofluorescence binding assay (Fig. 3). Anti-Rp5-L antiserum-stained Raji cells, causing a right shift in fluorescence compared with cells stained with anti-KLH antiserum (Fig. 3*A*). Preincubation of the antiserum with Rp15-C or unrelated peptide Qp-1a had no effect on the fluorescence intensity of the

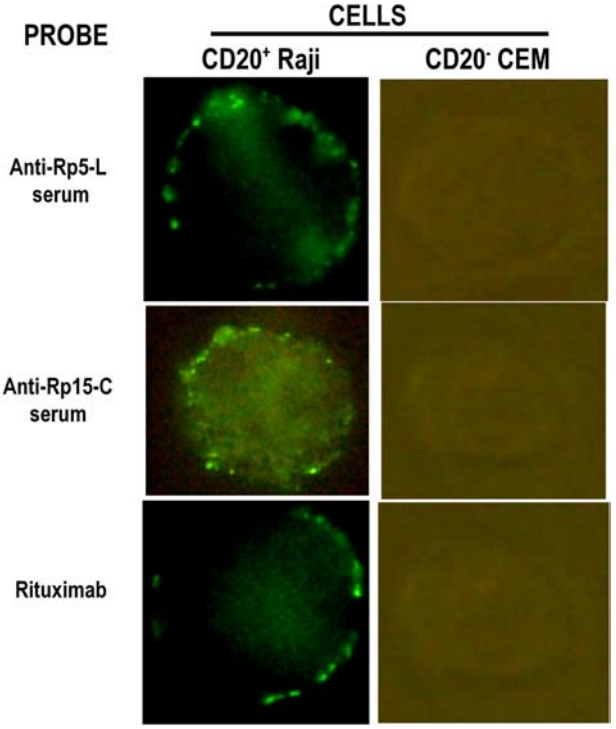

FIGURE 2. Anti-Rp5-L antiserum, like anti-Rp15-C antiserum and rituximab, stains $CD20^+$ cells with a punctate pattern indicative of CD20 localized in membrane raft microdomains. Anti-Rp5-L and anti-Rp15-C antisera (diluted 1/20 in PBS-BSA) and rituximab (2.5 μg/ml in PBS) were incubated with rabbit IgG-pretreated $CD20^+$ Raji or $CD20^-$ CEM cells (5×10^5 in 50 μl of PBS) for 30 min at 4°C. Cells were washed, labeled with FITC-conjugated anti-mouse or anti-human IgG (Fc portion), washed, fixed with paraformaldehyde, and examined by confocal microscopy at 488 nm. Data are representative of three independent experiments.

cells, whereas preincubation with increasing concentrations of the immunogenic peptide inhibited binding in a dose-dependent manner. Similarly, anti-Rp15-C antiserum, alone or in the presence of

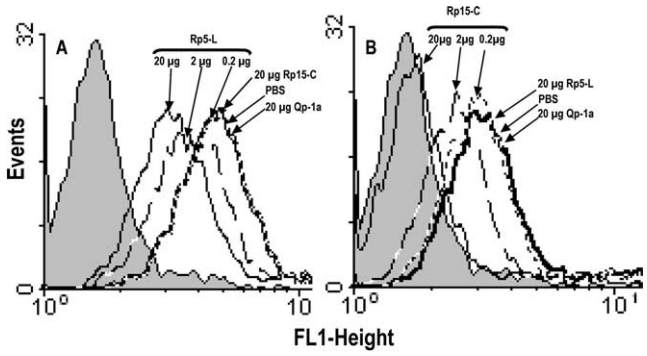

FIGURE 3. Rp5-L and Rp15-C induce anti-CD20 Abs that are specific to the immunogenic peptide only, without cross inhibition. Anti-Rp5-L (*A*) and anti-Rp15-C (*B*) antisera, diluted 1/20 in PBS-BSA, were preincubated with an equal volume of PBS containing 400, 40, or 4 μg/ml Rp5-L, Rp15-C, Qp-1a, or no peptide for 1 h at 4°C (400 μg/ml equals 254.4 μM Rp5-L, 385.2 μM Rp15-C, and 286.8 μM Qp-1a). The antiserum-peptide mixture was added to Raji cells (5×10^5) and incubated for 30 min at 4°C. Cells were washed and labeled with FITC-conjugated anti-mouse IgG (Fc portion). Immunofluorescence was measured on a FACScan cytofluorimeter. Cells incubated with anti-KLH antiserum (shaded area) and inhibition by unrelated peptide Qp-1a served as negative controls. This experiment was conducted three times with similar results. Twenty micrograms of Rp5-L, Rp15-C, and Qp-1a are 12.7, 19.3, and 14.4 nmol, respectively.

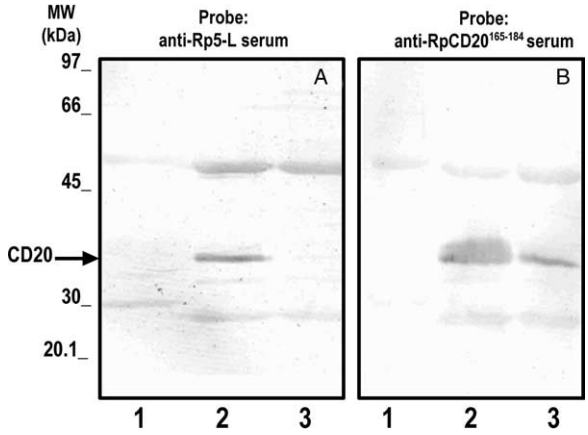

FIGURE 4. Anti-Rp5-L antiserum reacts with denatured CD20 immunoprecipitated with rituximab from $CD20^+$ Raji cell lysates. CD20 was immunoprecipitated from Raji cell lysates with rituximab, before and after preadsorption with rituximab. Immunoprecipitation with infliximab served as negative control. Immunoprecipitated proteins were separated on SDS-PAGE and revealed by Western blotting using anti-Rp5-L antiserum (*A*) or anti-RpCD20-L antiserum (*B*). *Lane 1*, Infliximab immunoprecipitates; *lane 2*, rituximab immunoprecipitates; *lane 3*, rituximab immunoprecipitates with prior preadsorption. Anti-Rp5-L specifically stained a band at 34 kDa, most likely to be CD20 because it was also stained by anti-RpCD20-L. The band at ~53 kDa is the H chain of rituximab. These results are representative of two different experiments.

unrelated peptides Rp5-L or Qp-1a, stained Raji cells with a right shift in fluorescence intensity; increasing concentrations of the immunogenic peptide inhibited this binding (Fig. 3*B*). The two antisera differed in the extent of inhibition by the corresponding peptide, as follows: 20 μg of Rp15-C (400 μg/ml, 385.3 μM) almost completely abolished the binding of anti-Rp15-C antiserum, but this same concentration of peptide Rp5-L (400 μg/ml, 254.5 μM) inhibited only ~40% of anti-Rp5-L antiserum binding. Furthermore, no cross-inhibition was observed: the highest concentration of peptide Rp5-L did not affect the reactivity of anti-Rp15-C antiserum, and vice versa.

Overall, these results indicate that anti-Rp5-L antiserum reacts specifically with CD20 in membrane raft microdomains, and that this reactivity is mediated by a specific interaction with the motif ⟨WPxWLE⟩. These results suggest that anti-Rp5-L and anti-Rp15-C antisera recognize different epitopes on CD20.

To further characterize the CD20 epitopes recognized by anti-Rp5-L and anti-Rp15-C antisera, we assessed their reactivity with denatured CD20 by Western blotting (Fig. 4). When CD20 was immunoprecipitated from Raji cells with rituximab, anti-Rp5-L antiserum stained a band with an apparent molecular mass of 34 kDa (Fig. 4*A*, *lane 2*). The reactivity was specific, because no staining was observed when cell lysates were immunoprecipitated with infliximab (*lane 1*) or extensively preadsorbed with rituximab before immunoprecipitation (*lane 3*). This 34-kDa band is likely to be CD20, because a similar band was detected when the rituximab immunoprecipitates were probed with anti-RpCD20-L antiserum (Fig. 4*B*). As expected, rituximab did not stain denatured CD20 (11), nor did anti-Rp15-C antiserum (data not shown). Thus, anti-Rp5-L (but not anti-Rp15-C or rituximab) recognizes a CD20 epitope that is not denatured during SDS-PAGE under reducing conditions. These results add further evidence to the hypothesis that anti-Rp5-L and anti-Rp15-C antisera recognize different epitopes on CD20.

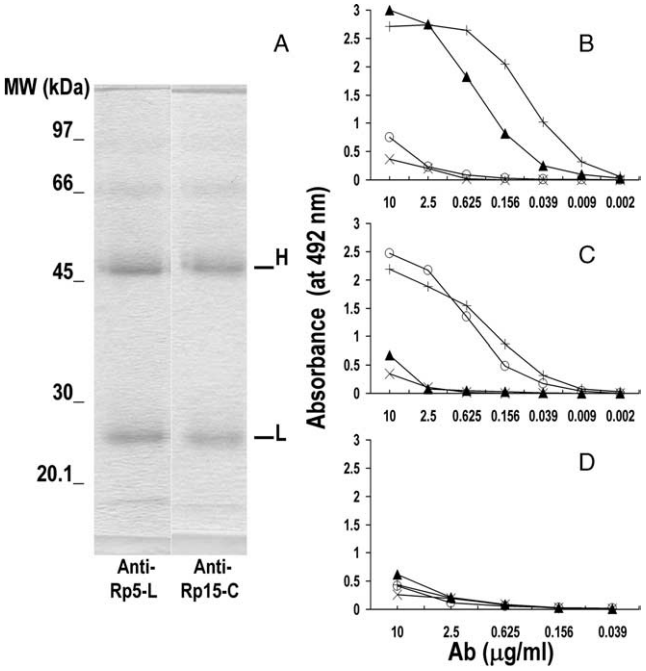

FIGURE 5. Antipeptide IgG from mice immunized with Rp5-L and Rp15-C maintain specificity for the immunogenic peptide only. *A*, Antipeptide IgG, purified from sera of immunized BALB/c mice and cleared of anti-KLH Abs, were separated on SDS-PAGE under reducing conditions (2 μg/lane) and stained with Coomassie brilliant blue. MW: m.w. markers. *B–D*, Ninety-six-well microtiter plates were coated with PBS containing 10 μg/ml KLH-conjugated Rp5-L (*B*), Rp15-C (*C*), or Qp-1a (*D*). Plates were washed; free protein-binding sites were blocked; and wells were treated with anti-Rp5-L IgG (▲), anti-Rp15-C IgG (○), rituximab (+), or infliximab (×) in 4-fold serial dilutions starting from 10 μg/ml. Following a 4-h incubation at 25°C and three washes, IgG-peptide interaction was detected with HRP-conjugated anti-mouse or anti-human IgG (Fc portion) and *o*-phenylenediamine. Absorbance was read at 492 nm. Background was determined from the absorbance in wells not coated with peptide. Each data point is the mean of duplicate wells (SEM < 10%). The data shown are representative of two experiments.

Anti-Rp5-L IgG do not recognize the motif ⟨ANPS⟩

To exclude the possibility that the different reactivities of anti-Rp5-L and anti-Rp15 Abs with denatured CD20 reflect different binding avidities, their fine specificities were analyzed at the molecular level. We reasoned that if Rp5-L conformationally mimics the CD20 ⟨ANPS⟩ epitope, then anti-CD20 Abs elicited with the linear peptide should also recognize ⟨ANPS⟩. Therefore, anti-Rp5-L and anti-Rp15-C IgG were purified (Fig. 5*A*) and tested for specificity in an ELISA. When ELISA plates were coated with KLH-conjugated Rp5-L (Fig. 5*B*), both rituximab and anti-Rp5-L IgG demonstrated saturable binding, whereas anti-Rp15-C and infliximab did not. Similarly, in Rp15-C-coated plates (Fig. 5*C*), both rituximab and anti-Rp15-C IgG showed saturable binding, but anti-Rp5-L and infliximab did not. The binding was specific, because none of these Abs bound plates coated with KLH-Qp-1a (Fig. 5*D*). These results demonstrate that the IgG generated by mice immunized with the two peptides maintain their distinct specificities.

To identify the motif recognized by anti-Rp5-L IgG, phage clones were isolated by panning the 7-mer cyclic and 12-mer PDPLs with anti-Rp5-L IgG. Of the 30 randomly selected colonies from the 12-mer PDPL, 24 (80%) specifically reacted with anti-Rp5-L IgG (Table I). Alignment of the nucleotide sequences of their peptide inserts revealed that 6 (25%) contained the same motif ⟨WPxWLE⟩ recognized by rituximab on the linear peptides (13). The consensus from all 24 inserts gave the immunogenic motif qWPxwL, similar to the antigenic motif. Panning of the 7-mer cyclic PDPL with anti-Rp5-L IgG did not result in the enrichment of any phage clones. This result suggests that Rp5-L does not mimic the conformational motif ⟨ANPS⟩, because phage clones expressing this motif were previously isolated from this library using rituximab (13) and anti-Rp15-C IgG (19).

Computer modeling of the Rp5-L motif ⟨WPxWLE⟩ and the CD20 ⟨ANPS⟩ motif bound to rituximab Fab

Considering the previously described immunochemical evidence that the Rp5-L motif ⟨**WPxWLE**⟩ is not a conformational mimic of the CD20 ⟨ANPS⟩ epitope, we used computer modeling to investigate contact points between the peptide and rituximab. To simplify the analysis, Rp5-L was replaced with the shorter Rp1-L (^{1}**WPRWLE**N^7). First, Rp1-L alone was modeled as a short α-helix (P^2-E^6) with the W^1 and W^4 indolic nuclei in parallel planes; the amino-terminal transactivation domain 2 of p53 (Brookhaven Protein Data Bank entry: 2GS0) was found as the template by SP4 algorithm. Then, Rp1-L was docked to rituximab Fab, and the pose with the highest ZDOCK score (1121.47) was chosen. As shown in Fig. 6*A*, Rp1-L docks with its N terminus inside the crevice of the

Table I. *Deduced amino acid sequences of the phage inserts isolated by panning with anti-Rp5-L IgG*

Immunogenic Peptide Bearing the Motif Recognized by Rituximab[a]		Phage Clones Isolated with Anti-Rp5-L Mouse IgG[b]				
				Specificity of reactivity ($A_{492\ nm}$)[c]		
Name	Sequence	PDPL	No. of positive clones (%)	Antipeptide IgG	Anti-KLH IgG	Deduced amino acid sequence[a,d]
Rp5-L	QDKLTQ**WP**K**WLE**	12-mer	5 (20.8)	2.2 ± 0.04	0.125 ± 0.2	QDKLTQ**WP**K**WLE**
			1 (4.2)	2.25	0.15	TTTTSV**WP**A**WLE**
			4 (16.7)	2.06 ± 0.02	0.084 ± 0.01	SVDQSY**WP**S**WL**D
			2 (8.3)	2.14 ± 0.1	0.13 ± 0.01	QVNPNQ**WP**R**WL**P
			11 (45.8)	2.15 ± 0.07	0.17 ± 0.27	Q**WP**SR**L**DRLERI
			1 (4.2)	2.05	0.04	TALQ**WP**TR**L**SGT
			Consensus			**qWPxwL**
		c7c-mer	0			

[a] Motif amino acids are shown in bold letters.
[b] Phage particles were isolated by panning, with purified anti-peptide IgG, the 12-mer linear (12-mer) and 7-mer cyclic (c7c-mer) PDPLs.
[c] Reactivity of phage particle supernatants with Abs, as measured by ELISA. Supernatants from phage particles expressing linear and cyclic peptides were diluted 8 and 32 times, respectively.
[d] Clones expressing sequences with the motif recognized by rituximab are underlined. Multiple alignments were performed with MULTALIN (http://npsa-pbil.ibcp.fr/cgi-bin/npsa_automat.pl?page=/NPSA/npsa_multalin.html).

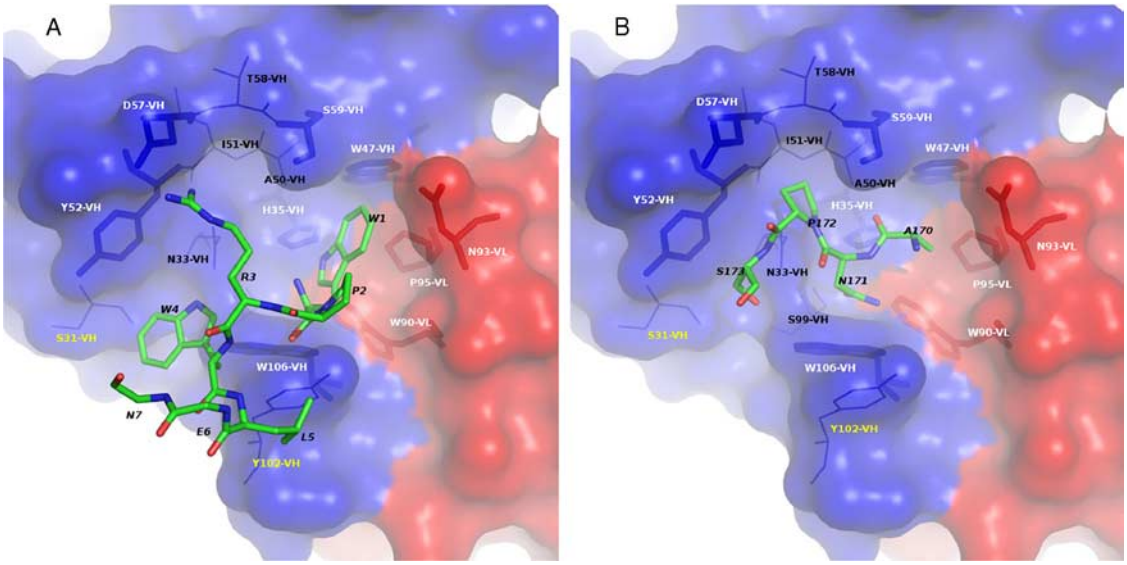

FIGURE 6. Computer modeling of the interaction between rituximab Fab and the Rp5-L motif ⟨^{1}WPxWLE^{7}⟩ (*A*) and comparison with that between rituximab Fab and ⟨^{170}ANPS^{173}⟩ of the extracellular loop of CD20 (*B*). *A*, Docking of Rp1-L (⟨^{1}WPRWLEN^{7}⟩), the shortest rituximab-specific peptide containing the same ⟨WPxWLE⟩ motif as Rp5-L, to rituximab Fab. Side chains of E^6 and N^7 are not shown for clarity. *B*, Docking of ⟨^{170}ANPS^{173}⟩ portion of CD20 to rituximab, according to the crystal structure of the complex (30). Rituximab Fab amino acids ($S^{31}{}_{VH}$ and $Y^{102}{}_{VH}$) preferentially involved in binding ⟨WPxWLE⟩ are labeled in yellow, those ($N^{33}{}_{VH}$, $A^{50}{}_{VH}$, $I^{51}{}_{VH}$, $T^{58}{}_{VH}$, and $S^{99}{}_{VH}$) preferentially involved in binding ⟨ANPS⟩ are in black, whereas rituximab Fab amino acids ($H^{35}{}_{VH}$, $W^{47}{}_{VH}$, $Y^{52}{}_{VH}$, $D^{57}{}_{VH}$, $S^{59}{}_{VH}$, $W^{106}{}_{VH}$, $W^{90}{}_{VL}$, $N^{93}{}_{VL}$, and $P^{95}{}_{VL}$) involved in binding both ⟨WPxWLE⟩ and ⟨ANPS⟩ are labeled in white and shown with heavy lines. Rituximab Fab H and L chains are colored in blue and red, respectively.

Fab pocket, whereas its C terminus (bearing the hydrophilic amino acids E^6 and N^7) remains outside. This position allows the following: 1) orthogonal σ-π–aromatic interactions of the peptide's W^1 with rituximab's $W^{47}{}_{VH}$, $W^{106}{}_{VH}$, and $W^{90}{}_{VL}$ and of the peptide's W^4 with rituximab's $W^{106}{}_{VH}$; 2) hydrogen bonding between the peptide's C-O backbone of W^1 with $Y^{102}{}_{VH}$; and 3) Van der Waals interactions between the peptide and rituximab involving P^2 and $Y^{102}{}_{VH}$, L^5, and $Y^{102}{}_{VH}$, as well as W^4 and $S^{31}{}_{VH}$, respectively.

The amino acids of rituximab modeled to interact with ⟨^{1}WPxWLE^{6}⟩ were compared with those known by crystallography to interact with the CD20 ⟨^{170}ANPS^{173}⟩ motif (Table II). The amino acids $W^{47}{}_{VH}$, $W^{90}{}_{VL}$, and $P^{95}{}_{VL}$ of the hydrophobic-aromatic area of the rituximab Fab, known as the main contact points for A^{170}, are also the contact sites of the peptide's W^1, whereas W^1 and W^4 (like Rp15-C N^{171}) interact with $W^{106}{}_{VH}$ of rituximab. In contrast, whereas $S^{31}{}_{VH}$ and $Y^{102}{}_{VH}$ preferentially interact with Rp1-L (Fig. 6*A*), $N^{33}{}_{VH}$, $A^{50}{}_{VH}$, $I^{51}{}_{VH}$, $T^{58}{}_{VH}$, and $S^{99}{}_{VH}$ interact only with ⟨ANPS⟩ (Fig. 6*B*).

Altogether, this analysis indicates that ⟨WPxWLE⟩ and ⟨ANPS⟩ share some contact sites within the rituximab Ag-combining site. Moreover, these results suggests that the two motifs have similar, yet not identical, tertiary interactions with rituximab.

Discussion

This investigation found that two structurally different rituximab-specific motifs, ⟨WPxWLE⟩ and ⟨ANPS⟩, contained in the linear

Table II. *Interactions between the motif ⟨WPxWLE⟩ and ⟨ANPS⟩ CD20 with rituximab Fab CDRs*

Fab-Rituximab Amino Acids[a]	Linear Peptide Motif Amino Acids						CD20 Motif Amino Acids			
	W1	P2	X3	W4	L5	E6	A170	N171	P172	S173
S31-VH				X						
N33-VH								X	X	**X**[b]
H35-VH	X						X	X		
W47-VH	X						X			
A50-VH									X	
ILE51-VH							X		X	
Y52-VH				X					X	X
D57-VH			**X**						X	
T58-VH									X	
S59-VH	X						X		X	
S99-VH								**X**		
Y102-VH	**X**			X	X					
W106-VH	X			X				**X**		
W90-VL	X						X			
N93-VL	X						X			
P95-VL	X						X			

[a] Contact is considered when the distance between any pair of heavy atoms is <4.0. Rituximab VL and VH chain amino acids with potential contact to both motif ⟨WPxWLE⟩ and ⟨ANPS⟩ are underlined.
[b] Amino acids of VL and VH forming H-bonding interactions are labeled with a bold cross.

peptide Rp5-L and the cyclic peptide Rp15-C (and in CD20 itself), respectively, are also conformationally different and are not replicas of a single CD20-associated epitope. In particular, we found that, like Rp15-C, Rp5-L mimics the raft-associated, functional form of CD20 and, in immunized mice, raises Abs that recognize this form of CD20. However, the antisera raised by the two peptides have different fine specificities for CD20, because no cross-inhibition was seen. Furthermore, anti-Rp5-L Abs recognized denatured CD20 in SDS-PAGE (anti-Rp15-C Abs and rituximab are known not to recognize denatured CD20). Finally, computer modeling of rituximab with the docked peptide indicated that some molecular contacts between rituximab and the two motifs are similar, whereas others are different.

The finding that Rp5-L is an effective mimotope of CD20 in the absence of primary sequence homology is not without precedent (13, 20, 21). In such cases, the peptide mimotope mimics a conformational or discontinuous epitope. In this study, immunochemical experiments and molecular modeling were used to investigate the mechanism by which the different motifs of Rp5-L and Rp15-C mimic CD20; three possibilities were considered, as follows: 1) Rp5-L conformationally mimics ⟨ANPS⟩; 2) Rp5-L and Rp15-C mimic different conformations of a single CD20 epitope; and 3) Rp5-L and Rp15-C mimic two distinct, but spatially close CD20 epitopes.

The first possibility is unlikely, because anti-Rp5-L Ab did not recognize the ⟨ANPS⟩ motif. In fact, binding of anti-Rp5-L antiserum to $CD20^+$ cells was not inhibited by Rp15-C, and PDPL panning with anti-Rp5-L IgG did not enrich phage clones expressing ⟨ANPS⟩-motif-containing peptides. These results indicate that the recognition of CD20 by anti-Rp5-L Abs is mediated by the specific reactivity with ⟨WPxWLE⟩, which is conformationally different from ⟨ANPS⟩.

The second possibility was based on the observation that CD20 changes conformation depending on the amount of membrane cholesterol (35) or during the transition from a weak to a strong raft-associated condition (24). Conformational changes of the CD20 epitope recognized by rituximab might be mimicked by two structurally different peptides. This possibility was excluded on the basis of their antigenic profiles, because both Rp5-L and Rp15-C inhibited the binding of rituximab to raft-associated CD20 as well as the rituximab-stimulated increase in ceramide. Furthermore, anti-Rp5-L Ab stained $CD20^+$ cells with a punctate pattern identical with that obtained with anti-Rp15-C Abs and rituximab, corresponding to the recognition of raft-associated CD20.

The third possibility is supported by the observation that, differently from anti-Rp15-C Abs that only recognize native (membrane-bound) CD20, anti-Rp5-L Abs also react with denatured CD20. This finding supports the possibility that Rp5-L and Rp15-C mimic two different epitopes of CD20.

The different specificities of the anti-peptide Abs may reflect differences between the motifs $\langle {}^{1}\text{WPXWLE}^{5}\rangle$ and $\langle {}^{170}\text{ANPS}^{173}\rangle$ in terms of the molecular interactions with rituximab, as evidenced by computer modeling of rituximab with docked peptide compared with the crystallographic structure of rituximab with bound CD20 (30). Both motifs fit reasonably well in the hydrophobic portion of the Ag-combining site of rituximab (residues $W^{47}{}_{VH}$, $Y^{102}{}_{VH}$, $W^{106}{}_{VH}$, $W^{90}{}_{VL}$, and $P^{95}{}_{VL}$), with some differences. First, the indolic group interactions between the peptide's W^1 and rituximab's $W^{47}{}_{VH}$, $W^{106}{}_{VH}$, and $W^{90}{}_{VL}$ and between the peptide's W^4 and rituximab's $W^{106}{}_{VH}$ force Rp1-L to be closer to this portion of the hydrophobic-aromatic pocket than CD20's ⟨ANPS⟩, which is more centered in the pocket, despite the fact that the side chains of A^{170} and N^{171} have hydrophobic and polar interactions with the same portion of the pocket. Second, the amino acids involved in the binding of the two motifs with rituximab are not identical: rituximab's $S^{31}{}_{VH}$ and $Y^{102}{}_{VH}$ interact only with $\langle {}^{1}\text{WPxWLE}^{5}\rangle$, whereas $N^{33}{}_{VH}$, $A^{50}{}_{VH}$, $I^{51}{}_{VH}$, $T^{58}{}_{VH}$, and $S^{99}{}_{VH}$ interact only with $\langle {}^{170}\text{ANPS}^{173}\rangle$.

This study has focused on cell lines that are established models to explore rituximab reactivity and/or function; hence, it is useful to evaluate how these are affected by mimotope peptides. Nonetheless, the inhibition of rituximab binding by Rp5-L (and Rp15-C) was also observed with other human B lymphoid cells (Ramos and LG-2) and with primary $CD20^+$ lymphocytes (data not shown). Moreover, an inhibitory effect in the human Burkitt's lymphoma cell line BJAB was recently reported for the Rp5-L-family peptide Rp10-L (bearing the Rp5-L motif ⟨WPxWLE⟩ (13, 16)), which competed with the binding of a rituximab-derived construct (36).

In the present study and in a previous investigation (19), we have shown that anti-CD20 Abs elicited by linear and cyclic rituximab-specific peptides recognize the same antigenic motif seen by rituximab, and we do expect these Abs to recognize any $CD20^+$ cell reacting with rituximab, including primary non-Hodgkin lymphoma B cells. Even so, the effective assessment of these Abs' reactivity with primary tumor B cells remains to be determined.

In our immunochemical experiments, we observed that the antipeptide antisera from immunized mice did not all react with CD20 (two of five animals immunized with either Rp5-L or Rp15-C developed anti-CD20 Abs). This variability of the immune response is surprising because the animals have the same genetic background (they are inbred and from the same colony). Nonetheless, it was expected based on our previous work (13, 19) and on similar observations with mimics of HLA (37) and other tumor-associated Ags (21, 38). The mechanism underlying these findings has not been elucidated. One possible, yet speculative, explanation for this phenomenon is the random occurrence of rearrangements in the V region of the BCR gene following immunization, which may influence the Ab specificity for amino acids not included in the peptide antigenic motif (19).

Based on our previous demonstration that the binding of anti-Rp5-L antiserum to $CD20^+$ cells was completely and specifically inhibited by rituximab Fab (13), the incomplete inhibition by Rp5-L of anti-Rp5-L Ab binding to $CD20^+$ cells seen in this study (40% at the highest concentration tested) may be interpreted in two ways. The avidity of binding of anti-Rp5-L Ab to CD20 may be higher than that to the peptide itself. Alternatively, when mice are immunized with this peptide, they may produce Abs to an epitope of CD20 that is different from that mimicked by Rp5-L (⟨WPxWLE⟩), according to the phenomenon of epitope spreading (39, 40). If the latter case is true, then the lack of reactivity of rituximab with denatured CD20 and its reactivity with ⟨WPxWLE⟩ suggest that the portion of anti-Rp5-L Abs recognizing denatured CD20 is generated by epitope spreading.

The molecular basis of epitope spreading has not been clearly elucidated. In the CD20 model, it may rely on the recognition by anti-Rp5-L Abs of motif amino acids different from the ⟨WPxWLE⟩ recognized by rituximab. In support of this possibility is our finding that ⟨WPxWLE⟩ was expressed by only 25% of the phage clones isolated by panning with anti-Rp5-L IgG. Irrespective of the mechanism responsible for epitope spreading, these data provide evidence that ⟨WPxWLE⟩ is the expression of a CD20 epitope structurally and conformational different from ⟨ANPS⟩ and that rituximab recognizes two different epitopes.

The functional significance of ⟨WPxWLE⟩ recognition remains to be determined. It may strengthen rituximab's binding once the mAb has reacted with ⟨ANPS⟩ in CD20, or alternatively, it may

favor the reactivity of rituximab to additional ⟨WPxWLE⟩-expressing molecules closely linked to CD20 in raft microdomains. The possibility that rituximab recognizes two distinct CD20 epitopes is reminiscent of recent findings by Teeling et al. (9), who investigated the fine specificity of a panel of fully human anti-CD20 mAbs generated in human Ig transgenic mice. They found that two distinct CD20-associated determinants were critical for mAb binding, as follows: the first (residues 146–173) was localized to the N-terminal side of the rituximab-specific motif ^{170}ANPS^{173}, whereas the second (residues 72–80) was found on the smaller extracellular loop. They proposed that this dual epitope recognition could account for the mAbs' slow-off rate and ability to activate complement (9). It remains to be determined whether this dual epitope recognition is also responsible for the relatively low rate of cellular internalization of bound rituximab (compared with mAb 1F5 (25), which only recognizes ⟨ANPS⟩ (13)) or for the ability of rituximab to reverse multidrug resistance (compared with mAb 1F5) (41), or is of importance in the therapeutic efficacy of rituximab. Ongoing experimentation with 64 Rp5-L-specific mAbs that do not react with ⟨ANPS⟩-bearing peptides will address this issue.

Besides providing insight, at the molecular level, into the mimicry by a linear peptide of a conformational epitope, this study suggests that linear and cyclic peptides may have different biological effects in the context of a vaccination strategy. Only clinical trials will determine whether the best therapeutic effects can be obtained by immunization with either cyclic or linear peptides, or with both.

Acknowledgments

We are grateful to Dr. Daniele Dell'Orco (Modena, Italy) for helpful suggestions in developing docking model, and to Vito Iacovizzi for his excellent secretarial assistance. Valerie Matarese provided scientific editing.

Disclosures

The authors have no financial conflict of interest.

References

1. Deans, J. P., H. Li, and M. J. Polyak. 2002. CD20-mediated apoptosis: signalling through lipid rafts. *Immunology* 107: 176–182.
2. Leget, G. A., and M. S. Czuczman. 1998. Use of rituximab, the new FDA-approved antibody. *Curr. Opin. Oncol.* 10: 548–551.
3. Coiffier, B. 2006. Monoclonal antibody as therapy for malignant lymphomas. *C. R. Biol.* 329: 241–254.
4. Cheson, B. D., and J. P. Leonard. 2008. Monoclonal antibody therapy for B-cell non-Hodgkin's lymphoma. *N. Engl. J. Med.* 359: 613–626.
5. Check, E. 2004. Mouse opens door for study of autoimmune diseases. *Nature* 428: 786.
6. Edwards, J. C., and G. Cambridge. 2006. B-cell targeting in rheumatoid arthritis and other autoimmune diseases. *Nat. Rev. Immunol.* 6: 394–403.
7. Bezombes, C., S. Grazide, C. Garret, C. Fabre, A. Quillet-Mary, S. Muller, J. P. Jaffrezou, and G. Laurent. 2004. Rituximab antiproliferative effect in B-lymphoma cells is associated with acid-sphingomyelinase activation in raft microdomains. *Blood* 104: 1166–1173.
8. Polyak, M. J., S. H. Tailor, and J. P. Deans. 1998. Identification of a cytoplasmic region of CD20 required for its redistribution to a detergent-insoluble membrane compartment. *J. Immunol.* 161: 3242–3248.
9. Teeling, J. L., W. J. Mackus, L. J. Wiegman, J. H. van den Brakel, S. A. Beers, R. R. French, M. T. van, S. Ebeling, T. Vink, J. W. Slootstra, P. W. Parren, et al. 2006. The biological activity of human CD20 monoclonal antibodies is linked to unique epitopes on CD20. *J. Immunol.* 177: 362–371.
10. Polyak, M. J., and J. P. Deans. 2002. Alanine-170 and proline-172 are critical determinants for extracellular CD20 epitopes; heterogeneity in the fine specificity of CD20 monoclonal antibodies is defined by additional requirements imposed by both amino acid sequence and quaternary structure. *Blood* 99: 3256–3262.
11. Ernst, J. A., H. Li, H. S. Kim, G. R. Nakamura, D. G. Yansura, and R. L. Vandlen. 2005. Isolation and characterization of the B-cell marker CD20. *Biochemistry* 44: 15150–15158.
12. Glennie, M. J., R. R. French, M. S. Cragg, and R. P. Taylor. 2007. Mechanisms of killing by anti-CD20 monoclonal antibodies. *Mol. Immunol.* 44: 3823–3837.
13. Perosa, F., E. Favoino, M. A. Caragnano, and F. Dammacco. 2006. Generation of biologically active linear and cyclic peptides has revealed a unique fine specificity of rituximab and its possible cross-reactivity with acid sphingomyelinase-like phosphodiesterase 3b precursor. *Blood* 107: 1070–1077.
14. Binder, M., F. Otto, R. Mertelsmann, H. Veelken, and M. Trepel. 2006. The epitope recognized by rituximab. *Blood* 108: 1975–1978.
15. Roberts, W. K., P. O. Livingston, D. B. Agus, J. Pinilla-Ibarz, A. Zelenetz, and D. A. Scheinberg. 2002. Vaccination with CD20 peptides induces a biologically active, specific immune response in mice. *Blood* 99: 3748–3755.
16. Perosa, F., E. Favoino, M. A. Caragnano, and F. Dammacco. 2005. CD20 mimicry by mAb rituximab-specific linear peptide: a potential tool for active immunotherapy of autoimmune diseases. *Ann. NY Acad. Sci.* 1051: 672–683.
17. Eisenberg, R., and R. J. Looney. 2005. The therapeutic potential of anti-CD20 "what do B-cells do?" *Clin. Immunol.* 117: 207–213.
18. Popa, C., M. J. Leandro, G. Cambridge, and J. C. Edwards. 2007. Repeated B lymphocyte depletion with rituximab in rheumatoid arthritis over 7 yrs. *Rheumatology* 46: 626–630.
19. Perosa, F., E. Favoino, C. Vicenti, F. Merchionne, and F. Dammacco. 2007. Identification of an antigenic and immunogenic motif expressed by two 7-mer rituximab-specific cyclic peptide mimotopes: implication for peptide-based active immunotherapy. *J. Immunol.* 179: 7967–7974.
20. Riemer, A. B., M. Klinger, S. Wagner, A. Bernhaus, L. Mazzucchelli, H. Pehamberger, O. Scheiner, C. C. Zielinski, and E. Jensen-Jarolim. 2004. Generation of peptide mimics of the epitope recognized by trastuzumab on the oncogenic protein Her-2/neu. *J. Immunol.* 173: 394–401.
21. Luo, W., J. C. Hsu, C. Y. Tsao, E. Ko, X. Wang, and S. Ferrone. 2005. Differential immunogenicity of two peptides isolated by high molecular weight-melanoma-associated antigen-specific monoclonal antibodies with different affinities. *J. Immunol.* 174: 7104–7110.
22. Wagner, S., C. Hafner, D. Allwardt, J. Jasinska, S. Ferrone, C. C. Zielinski, O. Scheiner, U. Wiedermann, H. Pehamberger, and H. Breiteneder. 2005. Vaccination with a human high molecular weight melanoma-associated antigen mimotope induces a humoral response inhibiting melanoma cell growth in vitro. *J. Immunol.* 174: 976–982.
23. Pashov, A. D., J. Plaxco, S. V. Kaveri, B. Monzavi-Karbassi, D. Harn, and T. Kieber-Emmons. 2006. Multiple antigenic mimotopes of HIV carbohydrate antigens: relating structure and antigenicity. *J. Biol. Chem.* 281: 29675–29683.
24. Li, H., L. M. Ayer, M. J. Polyak, C. M. Mutch, R. J. Petrie, L. Gauthier, N. Shariat, M. J. Hendzel, A. R. Shaw, K. D. Patel, and J. P. Deans. 2004. The CD20 calcium channel is localized to microvilli and constitutively associated with membrane rafts: antibody binding increases the affinity of the association through an epitope-dependent cross-linking-independent mechanism. *J. Biol. Chem.* 279: 19893–19901.
25. Michel, R. B., and M. J. Mattes. 2002. Intracellular accumulation of the anti-CD20 antibody 1F5 in B-lymphoma cells. *Clin. Cancer Res.* 8: 2701–2713.
26. Streicher, H. Z., F. Cuttitta, G. K. Buckenmeyer, H. Kawamura, J. Minna, and J. A. Berzofsky. 1986. Mapping the idiotopes of a monoclonal anti-myoglobin antibody with syngeneic monoclonal anti-idiotypic antibodies: detection of a common idiotope. *J. Immunol.* 136: 1007–1014.
27. Perosa, F., G. Luccarelli, M. Prete, E. Favoino, S. Ferrone, and F. Dammacco. 2003. β_2-microglobulin-free HLA class I heavy chain epitope mimicry by monoclonal antibody HC-10-specific peptide. *J. Immunol.* 171: 1918–1926.
28. Perosa, F., R. Carbone, S. Ferrone, and F. Dammacco. 1990. Purification of human immunoglobulins by sequential precipitation with caprylic acid and ammonium sulphate. *J. Immunol. Methods* 128: 9–16.
29. Liu, S., C. Zhang, S. Liang, and Y. Zhou. 2007. Fold recognition by concurrent use of solvent accessibility and residue depth. *Proteins* 68: 636–645.
30. Du, J., H. Wang, C. Zhong, B. Peng, M. Zhang, B. Li, S. Huo, Y. Guo, and J. Ding. 2007. Structural basis for recognition of CD20 by therapeutic antibody rituximab. *J. Biol. Chem.* 282: 15073–15080.
31. Mintseris, J., B. Pierce, K. Wiehe, R. Anderson, R. Chen, and Z. Weng. 2007. Integrating statistical pair potentials into protein complex prediction. *Proteins* 69: 511–520.
32. Dell'Orco, D., M. Seeber, P. G. De Benedetti, and F. Fanelli. 2005. Probing fragment complementation by rigid-body docking: in silico reconstitution of calbindin D9k. *J. Chem. Inf. Model* 45: 1429–1438.
33. Jo, S., T. Kim, V. G. Iyer, and W. Im. 2008. CHARMM-GUI: a web-based graphical user interface for CHARMM. *J. Comput. Chem.* 29: 1859–1865.
34. Thanos, C. D., W. L. DeLano, and J. A. Wells. 2006. Hot-spot mimicry of a cytokine receptor by a small molecule. *Proc. Natl. Acad. Sci. USA* 103: 15422–15427.
35. Polyak, M. J., L. M. Ayer, A. J. Szczepek, and J. P. Deans. 2003. A cholesterol-dependent CD20 epitope detected by the FMC7 antibody. *Leukemia* 17: 1384–1389.
36. Bremer, E., B. ten Cate, D. F. Samplonius, N. Mueller, H. Wajant, A. J. Stel, M. Chamuleau, A. A. van de Loosdrecht, J. Stieglmaier, G. H. Fey, and W. Helfrich. 2008. Superior activity of fusion protein scFvRit:sFasL over co-treatment with rituximab and Fas agonists. *Cancer Res.* 68: 597–604.
37. Perosa, F., and S. Ferrone. 1989. Murine antiidiotypic monoclonal antibodies that bear the internal image of HLA-DR allospecificities. *J. Clin. Invest.* 84: 907–914.
38. Srinivasan, R., A. N. Houghton, and J. D. Wolchok. 2002. Induction of autoantibodies against tyrosinase-related proteins following DNA vaccination: unexpected reactivity to a protein paralogue. *Cancer Immun.* 2: 8.
39. Vanderlugt, C. L., and S. D. Miller. 2002. Epitope spreading in immune-mediated diseases: implications for immunotherapy. *Nat. Rev. Immunol.* 2: 85–95.
40. Disis, M. L., V. Goodell, K. Schiffman, and K. L. Knutson. 2004. Humoral epitope-spreading following immunization with a HER-2/neu peptide based vaccine in cancer patients. *J. Clin. Immunol.* 24: 571–578.
41. Ghetie, M. A., M. Crank, S. Kufert, I. Pop, and E. Vitetta. 2006. Rituximab but not other anti-CD20 antibodies reverses multidrug resistance in 2 B lymphoma cell lines, blocks the activity of P-glycoprotein (P-gp), and induces P-gp to translocate out of lipid rafts. *J. Immunother.* 29: 536–544.